Dark Matter Search in Dwarf Irregular Galaxies with Ten Years of Data from the IceCube Neutrino Observatory

Yi-Fei Lü, Ben-Yang Zhu, Rong-Lan Li, Xue-Kang Guo, Tian-Ci Liu, Yong-Bo Huang, and Yun-Feng Liang
Guangxi Key Laboratory for Relativistic Astrophysics, School of Physical Science and Technology, Guangxi University, Nanning 530004, China
liangyf@gxu.edu.cn

Abstract

Dwarf irregular galaxies (dIrrs), as rotationally supported systems, have more reliable J-factor measurements than dwarf spheroidal galaxies and have received attention as targets for dark matter detection in recent years. In this paper, we use 10 yr of IceCube muon-track data and an unbinned maximum-likelihood-ratio method to search for neutrino signals beyond the background from the directions of seven dIrrs, aiming to detect neutrinos produced by heavy annihilation dark matter. We do not detect any significant signal. Based on such null results, we calculate the upper limits on the velocity-averaged annihilation cross section for 1 TeV–10 PeV dark matter. Our limits, although weaker than the strictest constraints in the literature in this mass range, are also a good complement to the existing results considering the more reliable J-factor measurements of dIrrs.

Key words: (cosmology:) dark matter – cosmology: theory – galaxies: dwarf

1. Introduction

Astrophysical and cosmological evidence has suggested the existence of particles beyond the Standard Model, dark matter (DM), which account for about 84% of the matter component of the universe (Planck Collaboration et al. 2016, 2020; Bertone & Hooper 2018; Arbey & Mahmoudi 2021). Although its nature is still unknown, many models, such as primordial black holes (PBH) (Carr & Kuhnel 2021), weakly interacting massive particles (WIMPs) (Bertone et al. 2005; Roszkowski et al. 2018), axion/axion-like particles (ALPs) (Saikawa 2017) and sterile neutrinos (Kopp 2021) are proposed as dark matter candidates. In recent years, most dark matter searches have focused on the mass range of the sub-eV (e.g., ALPs) or the GeV-TeV scale (e.g., WIMPs) and have not found a significant signal (Acharyya et al. 2023). The situation prompts us to consider the models in a wider mass range, one example is the ultra-heavy dark matter (UHDM).

The UHDM has a mass of above 10 TeV, which means it is too massive to be produced in current colliders. There are already many viable candidates for UHDM (Chung et al. 1998; Berlin et al. 2016a, 2016b; Kolb & Long 2017; Carney et al. 2022), and in this paper we focus on the annihilation UHDM which has received less attention before. In the scenario of thermal production of dark matter, the cross section of DM annihilation to Standard Model particles scales as M_χ^{-2} (Tak et al. 2022). As the mass increases, the cross section generally decreases. If it becomes too small, then the DM will not be sufficiently depleted before freeze-out, leading to an inconsistency with the observed cosmological DM density. This unitarity consideration limits the DM mass to be below

~100 TeV (Griest & Kamionkowski 1990; Bramante & Unwin 2017). Although this unitarity boundary has long hindered people's interest and enthusiasm in searching for the annihilation UHDM, several mechanisms have been proposed that can violate this boundary (Kim & Kuflik 2019; Carney et al. 2022). For instance, if the DM exists in a composite state rather than a point-like particle, thermal DM with PeV-scale masses could be possible (Harigaya et al. 2016; Tak et al. 2022). In such a scenario, the unitarity bound can be violated because the DM annihilation cross section no longer scales as M_χ^{-2}. Instead, it is now related to the geometric size of the composite DM.

One way to detect dark matter particles is to observe the gamma-rays, neutrinos from the DM annihilation or decay in the astrophysical environments. Promising sites for the observation of neutrinos from dark matter annihilation include the galaxy clusters, Galactic halo and center, as well as the cores of the Sun and Earth (Zornoza 2016). Among other targets, dwarf spheroidal galaxies (dSphs), one type of the Milky Way satellite galaxies, are also considered as promising objects because of their relatively close proximity and clean astrophysical background (Wood et al. 2015). However, the stellar kinematics of these pressure-supported galaxies are highly uncertain, which makes it difficult to determine their DM profiles very well (Battaglia et al. 2013). The accurate determination of the DM profile is very important for estimating astrophysical factor (J-factor) of DM indirect detection (Hayashi et al. 2016).

Dwarf irregular galaxies (dIrrs) are targets that we have paid less attention to Hernández Cadena et al. (2019), Abdallah et al. (2021),

Gammaldi et al. (2021), Alfaro et al. (2023), and they have some properties similar to dSphs, such as high DM abundance and low astrophysical background. Unlike dSphs, dIrrs are located further away and they are rotationally supported star-forming dwarf galaxies (Oh et al. 2015; Gammaldi et al. 2021) (in contrast, dSphs are pressure-supported systems). Their DM profiles can be obtained from their rotation curves. Meanwhile, dIrrs are in general larger galaxies compared to dSphs and have larger dark matter halos (their halo masses are $M_{200} = 10^7$–$10^{10} M_\odot$), and may host more DM subhalos (Karukes & Salucci 2017). The standard ΛCDM cosmological model predicts that dark matter halos are filled with many self-bound substructures, which has been confirmed by N-body simulations (Frenk & White 2012; Planck Collaboration et al. 2016). The presence of subhalos is expected to significantly enhance the DM signal (Lacroix et al. 2022; Runburg et al. 2022). Therefore, the enhancement factor due to subhalos increases the detectability of the dIrrs. These relevant properties make dIrrs also interesting targets for DM searches.

Previous works by IceCube collaboration, which have searched for dark matter signals from the Galactic center (Albert et al. 2020b; Iovine & IceCube Collaboration 2021), Galactic halo (Abbasi et al. 2023; Desai et al. 2023), Sun center (Argüelles et al. 2019; Abbasi et al. 2022), Earth center (Renzi 2019; Saveliev & Hyde 2022), and nearby galaxies and galaxy clusters (Aartsen et al. 2013a; Jeong et al. 2022), found no significant excess beyond background expectations. In our previous work, we have used IceCube observations on dwarf spheroidal galaxies to search for dark matter (Guo et al. 2023). In this paper, we further search for DM in dwarf irregular galaxies on the basis of the previous work. Different from the previous analysis, we analyze dwarf irregular galaxies as extended sources and consider the enhancement of the annihilation signal due to their internal subhalos. We will search for UHDM induced neutrinos from dIrrs using 10 yr (2008 April to 2018 July) of Icecube muon track data (IceCube Collaboration et al. 2021) and an unbinned maximum-likelihood-ratio method (Braun et al. 2008). We select seven dIrrs, four sources (WLM, NGC 6822, IC10, IC1613) are the most promising objects for DM detection as proposed in previous works (Gammaldi et al. 2018, 2021), and the remaining three sources are selected from (Alfaro et al. 2023). Note that the IceCube 10 yr muon track data have a much higher sensitivity to the northern hemisphere sky. Nevertheless, we have also included two sources in the southern sky (WLM and NGC 6822) in the sample to demonstrate this sensitivity difference. The sample information is shown in Table 1.

2. Signal Expectations

The expected differential neutrino flux for the annihilation of dark matter particles is calculated as follows:

$$\frac{d\Phi_\nu}{dE_\nu}(E_\nu) = \frac{\langle\sigma v\rangle}{8\pi m_\chi^2}\frac{dN_\nu}{dE_\nu}(E_\nu)J_{(\Delta\Omega)} \times B \tag{1}$$

where $\langle\sigma v\rangle$ is the velocity-averaged annihilation cross section, m_χ is the mass of the dark matter particle, dN_ν/dE_ν is the annihilation spectrum of DM particles, and B is the boost factor.

We assume dark matter annihilates into the standard model particles with a 100% branch ratio and calculate the energy spectrum of neutrinos dN_ν/dE_ν. For this calculation, we use the HDMSpectra (Bauer et al. 2021), a Python package providing spectra of various annihilation and decay channels of heavy dark matter. In this work, we consider the DM masses ranging from 1 TeV to 10 PeV and six annihilation channels: $b\bar{b}$, $t\bar{t}$, $\tau^+\tau^-$, $\nu_\mu\bar{\nu}_\mu$, $\mu^+\mu^-$ and W^+W^-. Figure 1 shows the neutrino spectra for the annihilation of a 100 TeV DM through different channels.

The flux is proportional to the J-factor (the integral over the square of the dark matter density),

$$J_{(\Delta\Omega)} = \int_{\Delta\Omega}\int_{\text{l.o.s}} dl\, d\Omega \rho_{\text{DM}}^2(r(l)) \tag{2}$$

where l is the distance along the line of sight (l.o.s.) and $r(l) = \sqrt{D^2 - 2lD\cos\theta + l^2}$ with D the distance to the source and θ the angular separation between the directions of the source center and l.o.s. In our work, we adopt the J-factors reported in (Alfaro et al. 2023).

The universal rotation curve model (Persic et al. 1996) can fit the dIrr rotation curve well (Gammaldi et al. 2018), and the DM distribution in these galaxies is well described by a Burkert profile (Burkert 1995):

$$\rho_{\text{DM}}(r) = \rho_0 \frac{r_0^3}{(r_0 + r)(r_0^2 + r^2)} \tag{3}$$

where ρ_0 is the normalization density, and r_0 is the core radius.

The substructures within dIrrs can increase the expected DM flux. We parameterize this effect with the boost factor B in Equation (1). For the calculation of the boost factors we mainly refer to the formulas and results in (Moliné et al. 2017). They considered the VL-II (Diemand et al. 2008) and ELVIS (Garrison-Kimmel et al. 2014, 2017) N-body cosmological simulations to study the properties of subhalos, obtaining the concentrations of the subhalos as a function of the distance R_{sub} to the main halo center. Together with the concentration-mass relation derived in (Pieri et al. 2011) for the field halo, we can calculate the luminosity $\mathcal{L}_{\text{smooth}}(M)$ of the smooth halo for a given halo mass M and the luminosity $\mathcal{L}_{\text{smooth}}(m, x_{\text{sub}})$ of the subhalo for a given halo mass m at the distance R_{sub} ($x_{\text{sub}} = R_{\text{sub}}/R_{\text{vir}}$ with R_{vir} the virial radius). Then the boost factor can be calculated with:

$$B(M) = \frac{3}{\mathcal{L}_{\text{smooth}}(M)}\int_{M_{\min}}^{M}\frac{dN(m)}{dm}$$
$$\times dm\int_0^1 dx_{\text{sub}}[1 + B(m)]\mathcal{L}(m, x_{\text{sub}})x_{\text{sub}}^2 \tag{4}$$

Table 1
Sample of dIrr Galaxies

Name	R.A. (deg)	Decl. (deg)	D (Mpc)	$\theta_{\rm vir}$ (deg)	σ_s (deg)	$\log_{10} J\,(\mathrm{GeV^2\,cm^{-5}})$	$\log_{10} M_{200}(M_\odot)$	Boost Factor	TS
IC10	5.10	59.29	0.79	3.857	0.078	17.857	10.6	5.53	0.04
IC1613	16.19	2.13	0.76	2.361	0.120	17.632	10.0	5.01	0.03
NGC 6822	296.23	−14.80	0.52	5.325	0.159	18.173	10.5	5.45	0.00
WLM	0.49	−15.46	0.98	2.609	0.082	18.062	9.6	4.72	0.00
DDO133	188.22	31.54	4.88	0.784	0.033	17.501	10.5	5.45	0.13
DDO154	193.52	27.15	4.04	0.695	0.030	17.800	10.3	5.25	0.00
DDO168	198.61	45.91	4.25	1.142	0.032	17.365	10.9	5.86	0.46

Note. Columns: (1) galaxy name (2) R.A. (3) decl. (4) galaxy distance (5) the angle to virial radii (6) source extension (7) the astrophysical factor for annihilation (8) halo mass (9) Boost Factor (10) TS value.
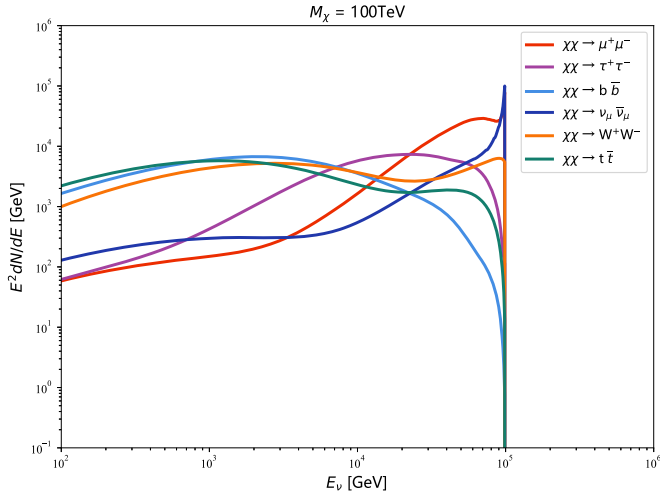

Figure 1. Spectra of neutrinos from the annihilation of DM particles with a mass of 100 TeV for six channels, assuming that the branching ratio for each channel is 100%.

The $dN(m)/dm$ is the subhalo mass function, which reads $dN(m)/dm = A/M(m/M)^{-\alpha}$. The normalization factor is equal to $A = 0.012$ for a slope of the subhalo mass function of $\alpha = 2$ and to $A = 0.03$ for $\alpha = 1.9$ (Sánchez-Conde & Prada 2014). It is important to note that there are large uncertainties in the calculation of the boost factor B(M), which depends on the index α of the mass function, the assumed minimum subhalo mass $M_{\rm min}$, the concentration-mass relation adopted for subhalos and whether or not the tidal stripping effect being taken into account. In this work, we adopt the median value of the boost factors reported in (Moliné et al. 2017): the mass function index is assumed to be 1.9, the minimum halo mass is $10^{-6} M_\odot$, and the tidal stripping effect is not considered. The boost factors are shown in Table 1.

3. Icecube Data Analysis

IceCube is a cubic-kilometer neutrino detector located at the South Pole. It consists of 5160 optical photosenors, which are connected to the data acquisition system via cables ("strings"). Neutrinos interact with nuclei and electrons in the ice producing charged particles and emitting Cherenkov light, which is detected by the photosensors (Aartsen et al. 2017b). The geometry and sensitivity of the photosensors lead to an effective low-energy threshold of about 100 GeV for neutrinos (Yoshida & IceCube Collaboration 2003).

In this work, we utilize the IceCube updated public data of muon tracks. This data set consists of muon tracks observed by IceCube from April 2008 to July 2018, including a total of 1134450 muon-track events. We use all IC40 to IC86-VII data, with the number in the name corresponding to the number of installed detector strings. The data include direction and energy information of neutrino events, as well as instrument response functions (IRFs, including effective area, smearing matrix, etc) for different periods over the ten years (IceCube Collaboration et al. 2021). We process the 19×2 double-counted tracks in the data set found in (Zhou & Beacom 2022), following the procedure in (Chang et al. 2022).[1]

The analysis is performed by using an unbinned maximum likelihood ratio method (Braun et al. 2008; Abbasi et al. 2011; Aartsen et al. 2013b, 2017a; Li et al. 2022; Pasumarti & Desai 2022). The likelihood function is defined as follows:

$$\mathcal{L}(n_s) = \prod_k \prod_{i=1}^{N^k} \left[\frac{n_s^k}{N^k} S_i^k + \left(1 - \frac{n_s^k}{N^k}\right) B_i^k \right], \qquad (5)$$

where S_i and B_i are the signal and background probability density functions (PDFs), respectively, N^k is the total number of events in the sample k and n_s^k is the number of signal events which is dependent on the model parameters. The superscript k refers to the kth IceCube data sample (IC40-IC86VII).

The signal and background PDFs for the ith event are functions of the reconstructed direction x_i and the reconstructed muon energy E_i. For time-integrated searches the signal PDF S_i

---

[1] See https://github.com/beizhouphys/IceCube_data_2008-2018_double_counting_corrected for the updated data set.

is given by:

$$S_i = S_i^{\text{spat}}(x_i, \sigma_i|x_s) \times S_i^{\text{ener}}(E_i|\gamma), \qquad (6)$$

where S_i^{spat} is the spatial contribution which depends on the angular uncertainty of the event σ_i and the angular separation between the directions of the event x_i and the source x_s. We model the spatial term of the signal PDF as a two-dimensional Gaussian,

$$S_i^{\text{spat}}(x_i, \sigma_i|x_s) = \frac{1}{2\pi\sigma_i^2} \exp\left(-\frac{|x_i - x_s|^2}{2\sigma_i^2}\right) \qquad (7)$$

where x_i is the direction of the ith event, and x_s is the direction to the source. Given the larger size of the dIrrs (compared to dSphs), it is better to analyze them as extended sources to get more realistic limits. In Table 1, we present the extension corresponding to the virial radius and the 68% containment angle of these dIrrs. When searching for an extended source, the value of σ_i is replaced with $\sigma = \sqrt{\sigma_i^2 + \sigma_s^2}$ (Aartsen et al. 2014; Albert et al. 2020a), where σ_s quantifies the extension of the source. In this work, we adopt the angle containing 68% of the total emission ($J_{(\sigma_s)} = 0.68 \times J_{\text{tot}}$) as σ_s (Geringer-Sameth et al. 2015; Di Mauro et al. 2022). The signal PDF becomes,

$$S_i^{\text{spat}} = \frac{1}{2\pi(\sigma_i^2 + \sigma_s^2)} \exp\left(-\frac{|x_i - x_s|^2}{2(\sigma_i^2 + \sigma_s^2)}\right). \qquad (8)$$

The energy term of the signal PDF, S_i^{ener}, is a function of the reconstructed muon energy proxy E_i. Assuming a power law spectrum of spectral index γ and for a given decl. δ_s of the source,[2] the PDF is (Huang & Li 2022),

$$S_i^{\text{ener}} = \frac{\int E_\nu^{-\gamma} A_{\text{eff}}^k(E_\nu, \delta_s) M_k(E_i|E_\nu, \delta_s) dE_\nu}{\int E_\nu^{-\gamma} A_{\text{eff}}^k(E_\nu, \delta_s) dE_\nu} \qquad (9)$$

For the search for DM signals, the $E_\nu^{-\gamma}$ should be replaced by a DM spectrum (i.e., Equation (1)).

The background PDF B_i is obtained directly from the experimental data and is given by

$$B_i^k = B_i^{\text{spat}}(\delta_i) \times B_i^{\text{ener}}(E_i|\delta_i) \qquad (10)$$

The spatial term, B_i^{spat}, is the normalized event number per unit solid angle and is varied with the decl. δ (Zhou et al. 2021),

$$B_i^{\text{spat}}(\delta_i) = \frac{N_{\delta_i \pm 3}^k}{N_k \times \Delta\Omega_{\delta_i \pm 3}} \qquad (11)$$

where $N_{\delta_i \pm 3}$ is the number of events in the decl. band of $\delta_i \pm 3$ and $\Delta\Omega_{\delta_i \pm 3}$ is its corresponding solid angle, N_k is the total number of events in the sample k. The background PDF is R.A.

---

[2] Considering the small extension of the dIrrs we are studying (see σ_s in Table 1), we disregard the variations of the IRFs within the region covered by the source, and adopt the instrument response toward the center of the source (α_s, δ_s).

independent because the IceCube observatory is located at the South pole.

The B_i^{ener} represents the energy term of the background PDF,

$$B_i^{\text{ener}}(E_i|\delta_i) = \frac{N_{ij}^k}{N_{\delta_i \pm 3}^k \Delta E} \qquad (12)$$

where N_{ij}^k is the number of events within the decl. range of $\delta \in [\delta_i - 3°, \delta_i + 3°)$ and the muon energy range of $\log_{10} E_{\text{rec}} \in [\log_{10} E_j, \log_{10} E_j + 0.1)$ for the sample k.

We maximize the likelihood in Equation (5) to derive the best-fit model parameters. A likelihood ratio test statistic of the signal is defined as,

$$\text{TS} = -2\log\left[\frac{L(\hat{n}_s)}{L(n_s = 0)}\right] \qquad (13)$$

where n_s is the number of signal events, and $\hat{n}_s$ is the best-fit value of the parameter.

For searching for DM signals, the number of signal neutrinos from DM annihilation in Equation (5) is related to the DM parameters through,

$$n_s = T_{\text{live}} \int_{E_{\text{min}}}^{E_{\text{max}}} A_{\text{eff}}(E_\nu, \delta) \frac{d\Phi_\nu}{dE_\nu}(E_\nu) dE_\nu \qquad (14)$$

where T_{live} is the detector uptime, A_{eff} is the effective area of the detector, $d\Phi_\nu/dE_\nu(E_\nu)$ is the energy spectrum of dark matter annihilating into neutrinos given by Equation (1), and the E_{min} and E_{max} are set to the minimum and maximum energies allowed by the effective area provided in the 10 yr IceCube data.

4. Result

Assuming a power-law spectrum, the TS values of the putative neutrino signals from these dIrrs are listed in Table 1. We do not find any significant excess beyond the background expectation in the directions of the seven sources within our sample. So we derive the flux upper limits at the 95% confidence level, assuming a source energy spectrum of E^{-2}, $E^{-2.5}$ and E^{-3}, respectively. The results are shown in Figure 2.

Next, we explore the neutrino signals from the annihilation of dark matter. We use Equation (1) to perform searches for the DM mass range from 1 TeV to 10 PeV and different annihilation channels, and find no annihilation signal. We calculate the upper limits at the 95% confidence level in the $\langle\sigma v\rangle - m_\chi$ parameter space for each dIrr. In Figure 3 we show the limits for the six annihilation channels ($b\bar{b}$, $t\bar{t}$, $\tau^+\tau^-$, $\nu_\mu\bar{\nu}_\mu$, $\mu^+\mu^-$, W^+W^-). The strongest constraints that we obtain are for the $\chi\chi \to \mu^+\mu^-$ channel.

In Figure 3, for the two southern sky sources, it can be seen that they place overall much weaker limits on the $\langle\sigma v\rangle$ than the dIrrs in the northern sky. However, at large DM masses ($\gtrsim 10^6$ GeV), they give stronger constraints. Such results are reasonable. In the southern hemisphere, since the event rate of
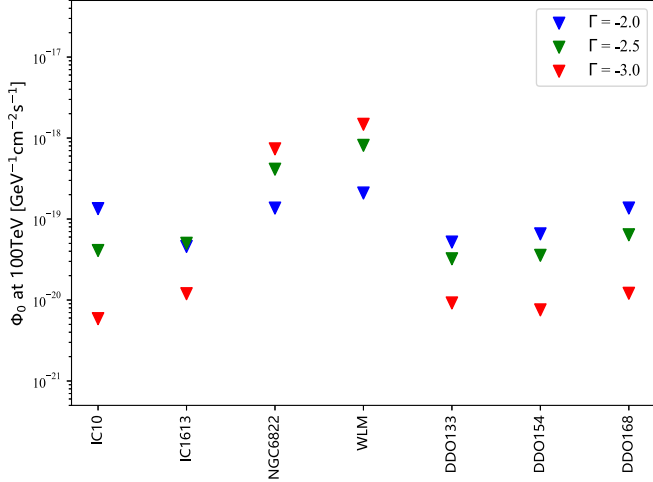
Figure 2. The 95% C.L. upper limits on the neutrino flux from the seven dIrrs at 100 TeV assuming a source spectrum of E^{Γ}.

atmospheric muons is orders of magnitude higher than that of neutrinos (Aartsen et al. 2017b), harsh cuts on the reconstruction quality and minimum energy are applied in order to suppress this atmospheric muon background, and the cuts remove most southern hemisphere events with an estimated energy below $\simeq 10$ TeV (IceCube Collaboration et al. 2021) (so for NGC 6822 and WLM we only show limits for DM masses of >10 TeV in Figure 3). In contrast, for the northern hemisphere, we can filter out the atmospheric muon contamination by the Earth. For neutrinos at the high-energy end ($>10^6$ GeV), on the other hand, events from the northern sky may interact far from the detector while crossing the Earth, resulting in unobservable energy losses and thus difficult to reconstruct. This leads to a significantly smaller effective area for the northern sky than the southern sky at $>10^6$ GeV energies (one can see Figure 2 of IceCube Collaboration et al. 2021). Since the energy spectra of the atmospheric muon and neutrino fluxes are expected to be softer than the astrophysical/ DM neutrinos, their contribution to the background becomes less significant at these high energies. Therefore, for the large mass DM, the analysis of the two dIrrs (NGC 6822, WLM) gives more strong constraints on the $\langle \sigma v \rangle$.

To improve the sensitivity, we also jointly analyze the data from the five northern-sky sources simultaneously. In this case, the combined likelihood function is

$$\widetilde{\mathcal{L}}(\langle \sigma v \rangle, m_\chi) = \prod_j \mathcal{L}_j(n_s(\langle \sigma v \rangle, m_\chi, J_j)) \qquad (15)$$

with $\mathcal{L}_j(n_s)$ the likelihood in Equation (5) for the jth source. The details of the method of the combined analysis can be found in (Guo et al. 2023; Zhu et al. 2023). The limits from the combined analysis are shown as black lines in Figure 3. The

results of the combined analysis are about 2.5 times stronger than the ones by DDO154, which gives the strongest constraints among the seven dIrr galaxies.

Finally, in Figure 4 we compare the results of this analysis with the limits obtained in other works (Aartsen et al. 2013a; Ackermann et al. 2015; Abdallah et al. 2021; Gammaldi et al. 2021; Miener et al. 2022; Acharyya et al. 2023; Alfaro et al. 2023). The combined limits are stronger than the results from the HESS observations of WLM dIrr (Abdallah et al. 2021) at the DM masses above 10 TeV. Compared to other results given by analyzing dSphs, it can be seen that our constraints are weaker, mainly owing to the fact that dwarf irregular galaxies are more distant and thus have smaller J-factors. The advantage of our results, however, is that the J-factors of dIrr galaxies can be more accurately determined compared to dSphs and the constraints are thus more robust, as they are rotationally supported galaxies. In contrast, as pressure-supported systems, dSphs have larger systematic uncertainties in the J-factor determination (Battaglia et al. 2013). However, for dIrrs, there exists another systematic uncertainty from the determination of the boost factor, as discussed in Section 2. For this reason, here we also present the upper limits given by the joint analysis when the boost factor is not taken into account, and the results are shown as dashed black lines in Figures 3 and 4.

From the individual constraints in Figure 3, we can see that the strength of the constraints depends mostly on the values of the dIrr J-factors, so the uncertainty of our results comes primarily from the J-factor uncertainty, which we discuss below. The (statistical) uncertainty on the dIrr J-factors includes mainly the error on the DM profile parameters obtained in the fit to the RC, which depends on the quality of kinematical measurements. This error is $\sim$15% for ρ_0 and r_0 and leads to a $\sim$75% uncertainty in the astrophysical J-factor (Gammaldi et al. 2018). In addition to this, there are some systematic uncertainties in the J-factor estimation, e.g., the choice of the model for the DM density profile causes a systematic uncertainty of $\sim$0.2 dex (Gammaldi et al. 2021). The J-factors used in this paper, which are derived in Gammaldi et al. (2018), assume a cored density distribution described by the Burkert profile (Burkert 1995), and such a profile is supported by the high-resolution HI observations (Oh et al. 2011, 2015) and can fit the rotation curves better (Gammaldi et al. 2021). However, DM-only N-body cosmological simulations favor a cuspy Navarro–Frenk–White profile (Navarro et al. 1997).

The largest uncertainty in the predicted DM annihilation flux comes from the uncertain nature of the dark matter substructure (i.e., the uncertainty in the enhancement factor B). As can be seen from Figure 4, whether the boost factor is considered or not, there is a factor of $\sim$5 difference in the results. In the case of considering the boost factor, different choices of the parameters of the subhalo population (e.g., the slope of the
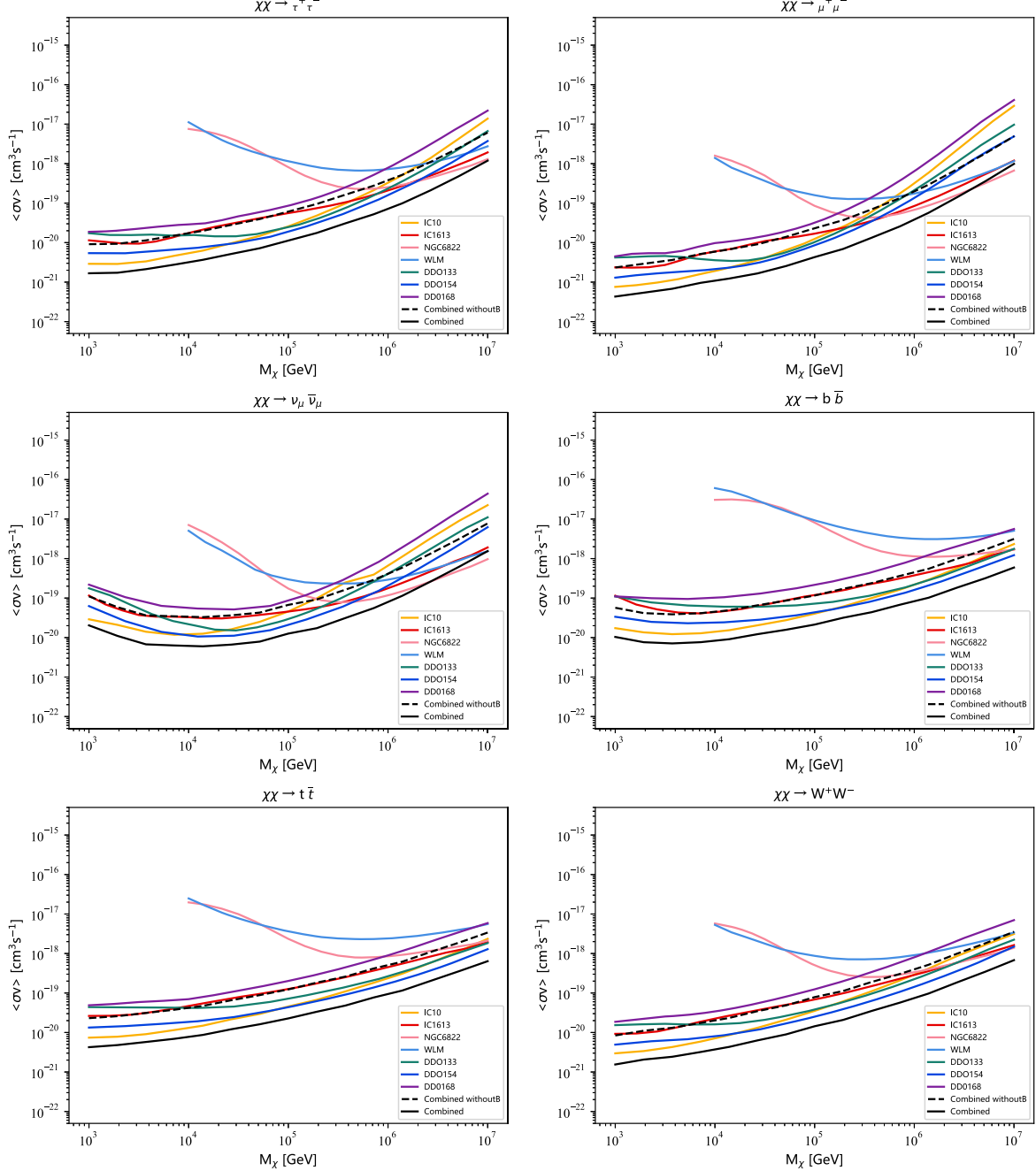
Figure 3. Upper limits on the DM annihilation cross section from the IceCube observations of dIrr galaxies for different channels. The black lines indicate the upper limits from the combined analysis of dIrrs. The two southern-hemisphere sources (WLM and NGC 6822) give weaker constraints especially in the lower mass regime.

subhalo mass function, the minimal subhalo mass) lead to distinct (boosted) J-factors, as has been discussed in Section 2 (see also Refs. Liang et al. 2017; Moliné et al. 2017; Gammaldi et al. 2021). Overall, for a dIrr of $10^{10} M_\odot$, the boost factor varies over a range of about 2.1–15.9 (Moliné et al. 2017), and thus the constraints (with B) on the DM parameters have the same level of uncertainty.

5. Conclusions

Pressure-supported dSphs are often considered as one of the most promising targets for indirect DM searches because of their close proximity and negligible astrophysical background. The problem, however, is that the DM content of dSphs and their astrophysical J-factors are usually subject to significant
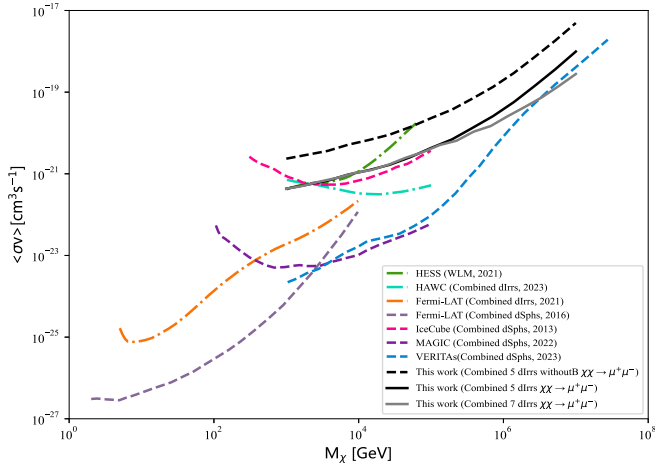
Figure 4. A comparison of our constraints (black solid and dashed lines) with other existing limits in the literature. The results plotted for comparison are based on the observations from IceCube (Aartsen et al. 2013a), Fermi-LAT (Ackermann et al. 2015; Gammaldi et al. 2021), HAWC (Alfaro et al. 2023), HESS (Abdallah et al. 2021), MAGIC (Miener et al. 2022) and VERITAS (Acharyya et al. 2023).

systematic errors due to their kinematic uncertainty. In contrast, dIrrs are rotationally supported dwarf galaxies, which are also DM-dominated objects. Unlike dSphs, the kinematics of dIrr galaxies provide a good estimate of their DM halo density distribution, and hence of their astrophysical J-factors. Although there exists certain star formation activity within dIrrs, it has been shown that the astrophysical background component is negligible (Gammaldi et al. 2018). They are therefore interesting novel targets for indirect detection of dark matter. In this work, we search for signals from UHDM annihilation in seven dIrrs using 10 yr of IceCube neutrino data. In the calculation of the J-factors of the dIrrs, we use a Burkert profile to characterize their DM distribution and consider the boost factors due to the existence of subhalos. Also, considering the angular extension of dIrr galaxies in the sky, we analyze them as extended sources.

We do not detect any significant signal of DM annihilation in the directions of these seven dIrrs. Based on the null results, we can place constraints on the model parameters of dark matter, since the emission from the annihilation should be detected if the annihilation cross section is large enough. Consequently, we derive the upper limits on the annihilation cross section at the 95% confidence level for the DM with masses between 1 TeV and 10 PeV. For the single-source analysis, the dIrr DDO154 gives the strictest exclusion limits. We also compute the results of the joint analysis of the five dIrrs in the northern sky. The joint analysis gives stronger (by a factor of 2–3) constraints on the annihilation cross section compared to the single-source analysis.

In contrast to other experimental results, our constraints are equivalent to those given by the HAWC observations of dIrrs (Alfaro et al. 2023) and stronger than the constraints from the HESS observations of the WLM dIrr (Abdallah et al. 2021). We also find that the exclusion limits of dIrrs are weaker than but close to those of dSphs (especially for the latest VERITAS results (Acharyya et al. 2023) at PeV masses), considering the smaller J-factor uncertainties of dIrrs, our results, therefore, provide a valuable complement to the existing results.

References

Aartsen, M. G., Abbasi, R., Abdou, Y., et al. 2013a, PhRvD, 88, 122001
Aartsen, M. G., Abbasi, R., Abdou, Y., et al. 2013b, ApJ, 779, 132
Aartsen, M. G., Abraham, K., Ackermann, M., et al. 2017a, ApJ, 835, 45
Aartsen, M. G., Ackermann, M., Adams, J., et al. 2017b, JInst, 12, P03012
Aartsen, M. G., Ackermann, M., Adams, J., et al. 2014, ApJ, 796, 109
Abbasi, R., Abdou, Y., Abu-Zayyad, T., et al. 2011, ApJ, 732, 18
Abbasi, R., Ackermann, M., Adams, J., et al. 2022, PhRvD, 105, 062004
Abbasi, R., Ackermann, M., Adams, J., et al. 2023, PhRvD, 108, 102004
Abdallah, H., Adam, R., Aharonian, F., et al. 2021, PhRvD, 103, 102002
Acharyya, A., Archer, A., Bangale, P., et al. 2023, ApJ, 945, 101
Ackermann, M., Albert, A., Anderson, B., et al. 2015, PhRvL, 115, 231301
Albert, A., André, M., Anghinolfi, M., et al. 2020a, ApJ, 892, 92
Albert, A., André, M., Anghinolfi, M., et al. 2020b, PhRvD, 102, 082002
Alfaro, R., Alvarez, C., Arteaga-Velázquez, J. C., et al. 2023, ApJ, 945, 25
Arbey, A., & Mahmoudi, F. 2021, PrPNP, 119, 103865
Argüelles, C. A., Kheirandish, A., Lazar, J., & Liu, Q. 2019, arXiv:1909.03930
Battaglia, G., Helmi, A., & Breddels, M. 2013, NewAR, 57, 52
Bauer, C. W., Rodd, N. L., & Webber, B. R. 2021, JHEP, 2021, 121
Berlin, A., Hooper, D., & Krnjaic, G. 2016a, PhLB, 760, 106
Berlin, A., Hooper, D., & Krnjaic, G. 2016b, PhRvD, 94, 095019
Bertone, G., & Hooper, D. 2018, RvMP, 90, 045002
Bertone, G., Hooper, D., & Silk, J. 2005, PhR, 405, 279
Bramante, J., & Unwin, J. 2017, JHEP, 2017, 119
Braun, J., Dumm, J., De Palma, F., et al. 2008, APh, 29, 299
Burkert, A. 1995, ApJL, 447, L25
Carney, D., Raj, N., Bai, Y., et al. 2022, arXiv:2203.06508
Carr, B., & Kuhnel, F. 2021, arXiv:2110.02821
Chang, P.-W., Zhou, B., Murase, K., & Kamionkowski, M. 2022, arXiv:2210.03088
Chung, D. J. H., Kolb, E. W., & Riotto, A. 1998, PhRvD, 59, 023501
Desai, K., Li, R., & Meighen-Berger, S. 2023, arXiv:2302.10542
Di Mauro, M., Stref, M., & Calore, F. 2022, PhRvD, 106, 123032
Diemand, J., Kuhlen, M., Madau, P., et al. 2008, Natur, 454, 735
Frenk, C. S., & White, S. D. M. 2012, AnPhy, 524, 507
Gammaldi, V., Karukes, E., & Salucci, P. 2018, PhRvD, 98, 083008
Gammaldi, V., Pérez-Romero, J., Coronado-Blázquez, J., et al. 2021, PhRvD, 104, 083026
Garrison-Kimmel, S., Boylan-Kolchin, M., Bullock, J. S., & Lee, K. 2014, MNRAS, 438, 2578
Garrison-Kimmel, S., Bullock, J. S., Boylan-Kolchin, M., & Bardwell, E. 2017, MNRAS, 464, 3108
Geringer-Sameth, A., Koushiappas, S. M., & Walker, M. 2015, ApJ, 801, 74
Griest, K., & Kamionkowski, M. 1990, PhRvL, 64, 615
Guo, X.-K., Lü, Y.-F., Huang, Y.-B., et al. 2023, PhRvD, 108, 043001
Harigaya, K., Ibe, M., Kaneta, K., Nakano, W., & Suzuki, M. 2016, JHEP, 2016, 151

Hayashi, K., Ichikawa, K., Matsumoto, S., et al. 2016, MNRAS, 461, 2914
Hernández Cadena, S., Gammaldi, V., Serna Franco, J., et al. 2019, ICRC, 36, 520
Huang, T.-Q., & Li, Z. 2022, MNRAS, 514, 852
IceCube Collaboration, Abbasi, R., Ackermann, M., et al. 2021, arXiv:2101.09836
Iovine, N. & IceCube Collaboration 2021, JInst, 16, C09009
Jeong, M., Abbasi, R., Ackermann, M., et al. 2022, ICRC, 37, 506
Karukes, E. V., & Salucci, P. 2017, MNRAS, 465, 4703
Kim, H., & Kuflik, E. 2019, PhRvL, 123, 191801
Kolb, E. W., & Long, A. J. 2017, PhRvD, 96, 103540
Kopp, J. 2021, arXiv:2109.00767
Lacroix, T., Facchinetti, G., Pérez-Romero, J., et al. 2022, JCAP, 2022, 021
Li, R.-L., Zhu, B.-Y., & Liang, Y.-F. 2022, PhRvD, 106, 083024
Liang, Y.-F., Xia, Z.-Q., Duan, K.-K., et al. 2017, PhRvD, 95, 063531
Miener, T., Nieto, D., Gammaldi, V., Kerszberg, D., & Rico, J. 2022, arXiv:2205.07055
Navarro, J. F., Frenk, C. S., & White, S. D. M. 1997, ApJ, 490, 493
Oh, S.-H., de Blok, W. J. G., Brinks, E., Walter, F., & Kennicutt, R. C. J. 2011, AJ, 141, 193
Oh, S.-H., Hunter, D. A., Brinks, E., et al. 2015, AJ, 149, 180
Pasumarti, V., & Desai, S. 2022, JCAP, 2022, 002

Persic, M., Salucci, P., & Stel, F. 1996, MNRAS, 283, 1102
Pieri, L., Lavalle, J., Bertone, G., & Branchini, E. 2011, PhRvD, 83, 023518
Planck Collaboration, Ade, P. A. R., Aghanim, N., et al. 2016, A&A, 594, A13
Planck Collaboration, Aghanim, N., Akrami, Y., et al. 2020, A&A, 641, A6
Renzi, G. 2019, ICRC, 36, 541
Roszkowski, L., Sessolo, E. M., & Trojanowski, S. 2018, RPPh, 81, 066201
Runburg, J., Baxter, E. J., & Kumar, J. 2022, JCAP, 2022, 023
Saikawa, K. 2017, in Proc. European Physical Soc. Conf. High Energy Physics. 5-12 July (Venice: EPS-HEP2017), 83
Moliné, Á., Sánchez-Conde, M. A., Palomares-Ruiz, S., & Prada, F. 2017, MNRAS, 466, 4974
Sánchez-Conde, M. A., & Prada, F. 2014, MNRAS, 442, 2271
Saveliev, M., & Hyde, J. 2022, PhRvD, 105, 083025
Tak, D., Baumgart, M., Rodd, N. L., & Pueschel, E. 2022, ApJL, 938, L4
Wood, M., Anderson, B., Drlica-Wagner, A., Cohen-Tanugi, J., & Conrad, J. 2015, ICRC, 34, 1226
Yoshida, S. & IceCube Collaboration 2003, ICRC, 3, 1369
Zhou, B., & Beacom, J. F. 2022, PhRvD, 105, 093005
Zhou, B., Kamionkowski, M., & Liang, Y.-f. 2021, PhRvD, 103, 123018
Zhu, B.-Y., Li, S., Cheng, J.-G., et al. 2023, PhRvD, 108, 083034
Zornoza, J. D. 2016, arXiv:1601.05691